Desalination and Water Treatment
www.deswater.com

doi: 10.1080/19443994.2014.942558

56 (2015) 875–893
October

Taylor & Francis
Taylor & Francis Group

CCD Series No-14: SWRO-CCD under fixed-pressure and variable flow compared with fixed-flow and variable pressure conditions

Avi Efraty

Desalitech Ltd, P.O. Box 132, Har Adar 90836, Israel; email: avi@desalitech.com

Received 21 February 2014; Accepted 29 June 2014

ABSTRACT

A theoretical model on the basis of the conceptual principles of closed circuit desalination (CCD) is explored in the present study for the performance assessment of the single-element seawater desalination reverse osmosis (SWRO) unit ME (E = SWC6-MAX) of near absolute energy efficiency without an energy recovery device (ERD) under fixed-pressure (FP) of variable flow compared with fixed-flow (FF) of variable pressure conditions. Performance simulations of same feed source (3.2% NaCl), sequence duration (9.01 min), recovery (60.3%), average flux (14.9 lmh), concentrate recycling flow (4.0 m^3/h), number of CCD cycles (10), and cycle period (0.90 min/cycle) under FP (65 bar) compared with FF (37.1–71.3 bar) conditions revealed the respective specific energy values (SE) of 2.177 and 1.792 kWh/m^3 with average permeate Total Dissolved Salts (TDS) of 574 and 464 ppm. The average SE sequential progression under FF conditions (1.234–1.792 kWh/m^3) compared with that under FP conditions (2.140–2.177 kWh/m^3) reveals the declined percent energy-saving mode of the former as function of increased recovery (R) in the order: 32.2% (R = 40%); 30.1% (R = 45%); 26.4% (R = 50%), 21.9% (R = 55%); and 17.7% (R = 60,3%). Since conventional SWRO desalination of Ocean seawater (~35,000 ppm TDS equivalent to ~3.2 NaCl) is normally being carried out with ~45% recovery, average flux near 15 lmh and an applied pressure around 65 bar using ERD, the findings of the current study suggest RO energy saving of 30.1% before accounting for ERD energy losses if the desalination is performed with SWRO-CCD under FF conditions. This conclusion is supported by the reported SE (2.46 kWh/m^3) for the conventional SWRO desalination plant in Australia compared with the extrapolated SE value for Ocean water (~1.70 kWh/m^3) from normalized experimental SWRO-CCD data with Mediterranean seawater. The average TDS of permeate projections during the batch sequence progression under FP (110–574 ppm) compared with FF (291–454 ppm) conditions reveals higher quality permeates by the former up to 54% recovery and thereafter, the preference of the latter mode. The observed inversion takes place due to rapidly declined flux under the FP conditions towards the end of the batch sequence which creates a fast rise in TDS per cycle manifested also by the average TDS.

Keywords: CCD; SWRO; Compact SWRO units; High recovery; Low SWRO energy

1. Introduction

Since the inception of the membrane-based technology for seawater desalination by reverse osmosis (SWRO) in the early 1960s of last century [1], this rapidly growing technology [2] has played a steadily increasing role in the supply of domestic water needs

in coastal regions worldwide and this trend is bound to continue in view of the growing global population and in light of the adverse climate changes inflicted by the intensified global "green-house" effects. Membrane-based technologies are also becoming important for the treatment of industrial effluents in order to enable the reuse of rescued water and also effect reduction of disposed brine effluents by costly procedures. The increased demand for SWRO desalination by energy-intensive processes led to the short- and long-term objectives [3,4] for the development of such processes with emphasis on reduced energy consumption, higher recovery, declined fouling, and lower installation costs. Energy accounts to some 35–60% of the desalination cost with more expensive electricity manifested by a larger cost fraction, and therefore, advanced SWRO techniques of lower energy requirements are of increased significance.

The conventional plug flow desalination (PFD) techniques for seawater (SWRO) and brackish water (BWRO) have remained essentially unchanged since inception [1] some 55 years, although major components (e.g. membranes, pumps, energy recovery device (ERD), etc.) have improved significantly and allow a near state-of-the-art performance. Compared with the widespread conventional PFD for seawater (SWRO-PFD) [5], the newly emerging closed circuit desalination (CCD) technology for seawater (SWRO-CCD) was reported [6–10] to afford high recovery irrespective of the number of elements per module, near-absolute energy efficiency without need for ERD, reduced fouling, and flexible operational conditions. In contrast with conventional SWRO-PFD [5], SWRO-CCD is based on different conceptual principles centered on a consecutive sequential batch process performed under fixed-flow (FF) of variable pressure conditions with concentrates recycled from outlet to inlet of modules and mixed with fresh pressurized feed. The theoretically projected and experimentally demonstrated SWRO-CCD results are highly consistent and reveal that near- and long-term future objectives of the desalination industry can be met already today by CCD.

The theoretical models and experimental results described thus far for the newly emerging SWRO-CCD technology pertain to desalination under FF and variable pressure conditions of constant net driving pressure (NDP). The present study explores a theoretical model SWR-CCD system and its performance with FF under variable pressure conditions (SWRO-CCD-FF) compared with fixed-pressure (FP) and variable flow conditions (SWRO-CCD-FP). The SWRO-CCD model explored is that of a single-element module configuration (ME) in light of its recent demonstration [11] of high-volume reduction effectiveness for difficult effluents with high silica content under open-circuit conditions of declined flux.

2. Single-element SWRO-CCD units for batch and consecutive sequential batch operation under fixed or variable pressure conditions

The schematic unit design depicted in Fig. 1 is a single-element batch unit for SWRO-CCD performance evaluation of SWRO-CCD under FP and variable flow conditions or under FF and variable pressure conditions, depending on the selected mode of operation. The apparatus comprises of a single element in a pressure vessel also containing a single spacer in front to increase the intrinsic volume of the closed circuit, thereby allowing a longer sequential period, a manifold to enable concentrate recycling from module outlet to its inlet by means of a circulation pump equipped with *vfd* means (CP-*vfd*) for controlled rate of cross flow, a high-pressure pump with *vfd* means (HP-*vfd*) for controlled pressure or flow rate of pressurized feed, check valve means (one-way valve—OWV), actuated valve means (AV) for brine replacement by fresh feed before batch sequence initiated, and a line outlet for permeate. The CCD theoretical model design (Fig. 1) performance simulations under FP and FF conditions are compared in reference to applied pressures, specific energy (SE), permeate Total Dissolved Salts (TDS), sequence time duration, flux, and NDP as function of the batch progression recovery and CCD cycles. In order to enable the obtainment of relevant comparative data during the SWRO-CCD theoretical model evaluation study under FP and FF conditions, simulations are performed with the same feed solution (3.2% w/w NaCl), average flux (14.9 lmh), and cross-flow (4.0 m^3/h) of CP of fixed cycle duration (0.90 min/cycle), using the same membrane element (SWC6-MAX) [12] in the same apparatus (Fig. 1). The comparative model analysis under review pertains to batch processes of near-absolute energy efficiency without ERD means. The

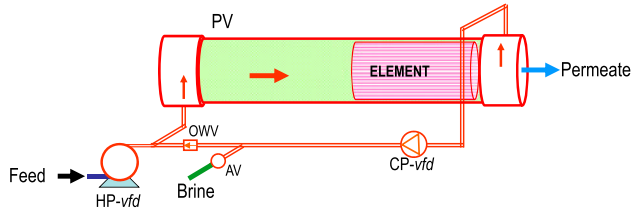

Fig. 1. A single-element apparatus of ME (E = SWC6-MAX) configuration for batch CCD comprising a single-element module (8´´) inside a single-pressure vessel also contains a single-element spacer, a HP-vdf, a CP-vdf, and actuated valve (AV) and check valve (OWV) means.

comparative results of this model analysis at the batch sequence level should also apply to the related consecutive sequential batch processes in the apparatus displayed in Fig. 2; wherein, brine replacement by fresh feed in continuous processes under FP or FF conditions takes place through a side conduit (SC). Replacement of brine by fresh feed without stopping desalination takes place by the engagement between the compressed, SC with fresh feed and the closed circuit, the SC with brine is then disengaged, decompressed, charged with fresh feed at near atmospheric pressure, compressed and left on standby for the next engagement. The operation of the unit with the SC (Fig. 2) proceeds with near-absolute energy efficiency since the compression/decompression steps take place under hydrostatic pressure conditions of negligible energy requirements.

3. Theoretical model database and simulation for the ME (E = SWC6-MAX) unit performance under FP and variable flow conditions with 3.2% NaCl feed

The theoretical model database for CCD-SWRO performance simulation furnished in Table 1 is for the ME (E = SWC6-MAX) unit design displayed in Fig. 1 under fixed applied pressure (65 bar) and variable flow conditions at 25˚C starting with flux of 50.5 lmh created by module recovery (MR) of 34% with fixed recycled cross-flow by CP (4.0 m^3/h) and fixed cycle duration (0.9 min/cycle) using a feed source of 3.2% NaCl equivalent to typical ocean seawater of 35,000 ppm. The selected starting flux (~50.5 lmh) and permeate flow (~2.06 m^3/h) are those of the SWC6-MAX membrane [12] test conditions, which in the context of the model simulation, requires MR = 34%, a value validated by an IMS Design Program (e.g. permeate = 2.1 m^3/h; MR = 33%; pressure = 63.5 bar; and beta = 1.15). The simulation database in Table 1 is shown at the top of the table with yellow background referring to the selected design features and operational conditions. Simulated CCD performance of said model system is carried per cycle with MR of each cycle selected to manifest the same desired applied pressure (e.g. 65 bar). The columns in the table are labeled at the bottom (A1–A30) and the content of each is explained hereinafter. Columns A1 and A2 stand for the mode of operation (CCD) and the CCD cycle number in the sequential batch process, respectively. The entire batch sequence in the model under review consists of 10 CCD cycles in succession. Columns A3, A4, and A5 describe the inlet, outlet, and mean-module concentrations, respectively, per each given CCD cycle derived from the selected MR for 65 bar applied pressure and the specified flow rates of the HP and CP pumps. Columns A6, A7, and A8 stand for the inlet, outlet, and average osmotic pressures, respectively, per each given CCD cycle derived from the appropriate module concentrations. Columns A9, A10, A11, and A12 stand for the flow rates of HP (Q_{HP}), CP (Q_{CP}), permeate (Q_P), and HP + CP (Q_{HP} + Q_{CP}, module inlet), respectively, per each given CCD cycle with that of CP maintained constant throughout the entire sequence, and those of HP and permeate change as a function of MR. Columns A13, A14, and A15 stand for the selected MR for 65 bar applies pressure and the calculated *pf* and applied pressure terms, respectively, with MR defined by Eq. (1) from the indicated flow rates adjusted per each cycle in compliance with the fixed applied pressure (65 bar) requirements expressed by Eq. (2) and *pf* expressed by Eq. (3); wherein, p_a stands for applied pressure (bar), μ for flux (lmh); A for permeability coefficient (l/m^2/h/bar); T_{CF} for temperature correction factor; $\Delta\pi_{av}$ for average module concentrate-side osmotic pressure (bar); Δp for pressure difference (bar) of CP; p_P for permeate release pressure (bar); π_P for module permeate-side osmotic pressure (bar); Y for MR ratio; and k for an empirical factor determined from the IMS design data for SWC6-MAX. Columns A16 and A17 stand for the declined sequential flux per cycle and the sequence average, respectively. Incidentally, the NDP which dictates the declined flux conditions in the said process is determined from the relevant listed parameters in Eq. (4). Columns A18 and A19 stand for CCD Cycle-Duration (CD) and cumulative sequential time progression (Σmin), respectively, the former expressed in minute/cycle by Eq. (5); wherein, Q_{CP} (m^3/h) stands for the cross-flow rate of CP (4.0 m^3/h) and V_i for the intrinsic volume of the closed circuit (60.1 liter) and the

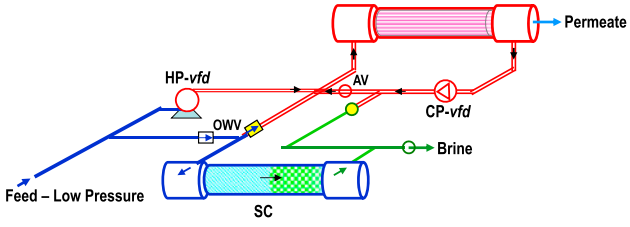

Fig. 2. A single-element apparatus of ME (E = SWC6-MAX) configuration for continuous consecutive sequential batch operation comprising a single module with a single element (8´´), HP-*vdf*, CP-*vdf*, Side-Conduit (SC), and actuated valve (AV) and check valve (OWV) means to enable the engagement/disengagement of the SC with the closed circuit of the unit. The figure illustrates the mode of actuation with SC disengaged from with the closed circuit for replacement of decompressed brine with fresh feed without stopping the desalination.

Table 1
Theoretical model simulation database of a single-element (SWC6-MAX) SWRO-CCD unit (Fig. 1) operation at 25°C under fixed applied pressure (65 bar) of declined flux starting at 50.5 lmh with MR of 34% and constant circulation flow (4.0 m^3/h) using feed of 3.2% NaCl equivalent to typical Ocean seawater of 35,000 ppm

TEST - SWC6 MAX		UNIT DESIGN		OPERATIONAL PARANETERS	
40.8	m2/Element	1	Modules	3.20	% NaCl Feed
50	m3/day	1	Elements/Module	0.85	Efficiey fator of HP
32,000	ppm NaCl	230	cm long PV	0.70	Efficiey fator of CP
54	bar Applied Pressure	20	cm diameter PV	0.20	bar -Δp CP
10	% Recovery	15	liter element volume	4.00	m3/h - CP
25	Centigrade.	5	% lines volume		
99.70	% Salt Rejection	60.1	liter per module	65.0	bar - Constant pressure
28.4	bar NDP			0.90	min/cycle
51.062	l/m2/h Flux	π(bar)-C(%)			
1.798	l/m2/h/bar -A	3.20	% NaCl Feed		
0.1203	l/m2/h - B	25.60	bar Osmotic Pressure		
		8.00	π(bar)/C(%)		

Process		Concentrations			Osmotic Pressures			Flow Rates				MR, *pf* and Pressure			Flux	
Mode	Cycle No	Inlet %	outlet %	mean %	Inlet barr	outlet bar	average bar	HP m3/h	CP m3/h	PERM m3/h	HP+CP m3/h	MR %	*pf* factor	Calcul. bar	Cycle lmh	av lmh
CCD	1	3.200	4.848	4.024	25.6	38.8	32.2	2.06	**4.00**	2.06	6.06	**34.00**	1.147	65.0	50.51	50.51
CCD	2	4.423	5.961	5.192	35.4	47.7	41.5	1.39	4.00	1.39	5.39	**25.80**	1.110	65.0	34.09	42.30
CCD	3	5.442	6.702	6.072	43.5	53.6	48.6	0.93	4.00	0.93	4.93	**18.80**	1.079	65.0	22.70	35.76
CCD	4	6.236	7.193	6.715	49.9	57.5	53.7	0.61	4.00	0.61	4.61	**13.30**	1.055	65.0	15.04	30.58
CCD	5	6.830	7.513	7.171	54.6	60.1	57.4	0.40	4.00	0.40	4.40	**9.10**	1.037	65.0	9.81	26.43
CCD	6	7.246	7.725	7.485	58.0	61.8	59.9	0.26	4.00	0.26	4.26	**6.20**	1.025	65.0	6.48	23.10
CCD	7	7.535	7.865	7.700	60.3	62.9	61.6	0.18	4.00	0.18	4.18	**4.20**	1.017	65.0	4.30	20.42
CCD	8	7.734	7.957	7.846	61.9	63.7	62.8	0.12	4.00	0.12	4.12	**2.80**	1.011	65.0	2.82	18.22
CCD	9	7.872	8.016	7.944	63.0	64.1	63.6	0.07	4.00	0.07	4.07	**1.80**	1.007	65.0	1.80	16.39
CCD	10	7.958	8.055	8.006	63.7	64.4	64.1	0.05	4.00	0.05	4.05	**1.20**	1.005	65.0	1.19	14.87
A1	**A2**	**A3**	**A4**	**A5**	**A6**	**A7**	**A8**	**A9**	**A10**	**A11**	**A12**	**A13**	**A14**	**A15**	**A16**	**A17**

Table 2 - contiinued

Process		Sequence Time, Permeate Volume, Recvoery & TDS							HP+CP: Power, Energy & Specific Energy					Permeate
									per Cycle			per Sequence		av Flow
Mode	Cycle No	Cycle min	Total ?min	Cycle liter	ΣV liter	Recovery %	Cycle ppm	average ppm	kW	kWh	k/Wh/m3	ΣkWh	kWh/m3	m3/h
CCD	1	0.90	0.90	30.95	31.0	34.0	109.9	110	4.410	0.0662	2.140	0.066	2.140	2.06
CCD	2	0.90	1.80	20.89	51.8	46.3	203	148	2.988	0.0449	2.149	0.111	2.143	1.73
CCD	3	0.90	2.70	13.91	65.8	52.3	347	190	2.000	0.0300	2.159	0.141	2.147	1.46
CCD	4	0.90	3.60	9.22	75.0	55.5	567	236	1.336	0.0201	2.177	0.161	2.151	1.25
CCD	5	0.90	4.51	6.01	81.0	57.4	912	286	0.882	0.0132	2.203	0.174	2.154	1.08
CCD	6	0.90	5.41	3.97	85.0	58.6	1,425	339	0.593	0.0089	2.244	0.183	2.159	0.94
CCD	7	0.90	6.31	2.63	87.6	59.3	2,192	395	0.404	0.0061	2.307	0.189	2.163	0.83
CCD	8	0.90	7.21	1.73	89.3	59.8	3,380	453	0.277	0.0042	2.401	0.194	2.168	0.74
CCD	9	0.90	8.11	1.10	90.4	60.1	5,356	513	0.188	0.0028	2.558	0.196	2.172	0.67
CCD	10	0.90	9.01	0.73	91.2	60.3	8,127	574	0.135	0.0020	2.778	0.198	2.177	0.61
A1	**A2**	**A18**	**A19**	**A20**	**A21**	**A22**	**A23**	**A24**	**A25**	**A26**	**A27**	**A28**	**A29**	**A30**

latter expressed by Eq. (6); wherein, N is the number of the specified cycle in the sequence. Noteworthy that CD is maintained fixed (0.90 min/cycle) throughout the sequence since both terms Q_{CP} and V_i remain unchanged.

Column A20 stands for permeate volume production at a specific cycle ($V_p(N)$-liter) expressed by Eq. (7) and column A21 for cumulative sequential permeate volume ($\Sigma V(N)$) over 1 → N cycles expressed by Eq. (8). Column A22 expresses the progressing sequence

recovery according to Eq. (9). Permeate TDS per cycle in column A23 is derived by Eq. (10); wherein, C_P stands for permeate TDS, C_f for feed TDS at start of each cycle, and B for the salt diffusion coefficient of the SWC6-MAX element. The TDS of permeates in column A24 is the average value at cycle N, and the preceding cycles which take account for the overall mass balance of produced permeates. The power (kW) requirements per cycle in column A25 are of HP plus CP as defined by the respective expressions Eqs. (11) and (12) with the cited parameters of flow rates (m^3/h), pressures (bar), and efficiency ratio of pumps (f). The module pressure difference term (Δp) in Eq. (12) is derived by Eq. (13); wherein, $n = 1$ stands for a single-element module, Q_{mi} ($=Q_P + Q_{CP}$) for module inlet flow rate, and Q_{mo} ($=Q_{CP}$) for module outlet flow rate and this approach gives consistent results with those of the IMS Design Program for SWC6-MAX. The energy (kWh) consumed per cycle in column A26 is the product of power and cycle time duration (CD), and column A27 discloses the SE per cycle on the basis of the energy consumed and permeate volume produced. Column 28 specifies the sequence energy accumulation (ΣkWh) and column 29 discloses the SE sequential progression according to Eq. (14) from the cited ΣkWh and ΣV terms. The final column 30 discloses the average sequential permeate production rate under the sequentially declined flux conditions.

$$\begin{aligned}\mathrm{MR}(\%) &= 100 \times Q_{HP}/(Q_{HP} + Q_{CP}) \\ &= 100 \times Q_P/(Q_P + Q_{CP})\end{aligned} \tag{1}$$

$$p_a = \mu/A/T_{CF} + \Delta\pi_{av} + \Delta p/2 + p_p - \pi_p \tag{2}$$

$$pf = 10^{(k \times Y)} \tag{3}$$

$$\mathrm{NDP} = p_a - \Delta\pi_{av} - \Delta p/2 - p_p + \pi_p \tag{4}$$

$$\mathrm{CD}(\mathrm{minute/cycle}) = (60/1,000) \times V_i/Q_{CP} \tag{5}$$

$$\Sigma\mathrm{min} = (60/1,000) \times V_i \times N/Q_{CP} \tag{6}$$

$$V_p(N) = [1,000/60] \times Q_p(N) \times \mathrm{CD} = Q_p(N) \times V/Q_{CP} \tag{7}$$

$$\begin{aligned}\Sigma V(N) &= V_p(N) + V_p(N-1) + V_p(N-2) + \cdots \\ &\quad + V_p(N=1)\end{aligned} \tag{8}$$

$$\text{Sequence recovery} = \Sigma V/(\Sigma V + V_i) \times 100 \tag{9}$$

$$C_p = B \times C_f \times pf \times T_{CF}/\mu \tag{10}$$

$$\begin{aligned}P_{HP}(\mathrm{kW})) &= (1/36) * Q_{HP} \times p_a/f_{HP} \\ &= (1/36) \times Q_P \times p_a/f_{HP}\end{aligned} \tag{11}$$

$$P_{CP}(\mathrm{kW}) = (1/36) \times Q_{CP} \times \Delta p/f_{CP} \tag{12}$$

$$\Delta p = (8/1,000) \times n \times [(Q_{mi} + Q_{mo})/2]^{1.7} \tag{13}$$

$$\text{Specific energy}\left(\mathrm{kWh/m^3}\right) = \Sigma\mathrm{kWh}/\Sigma\mathrm{V}\left(\mathrm{m^3}\right) \tag{14}$$

Parameter variations as function of sequential CCD cycles and batch recovery from the theoretical model performance simulation of the single element designed (Fig. 1) SWRO-CCD unit under fixed applied pressure (65 bar) and variable flow conditions with 3.2% NaCl feed according to the data in Table 1 are displayed in Figs. 3–12 in reference to concentrations (Fig. 3), osmotic pressures (Fig. 4), NDP (Fig. 5), flow rates (Fig. 6), flux (Fig. 7), MR (Fig. 8), concentration polarization (Fig. 9), TDS of permeates (Fig. 10), SE (Fig. 11), and permeate production rate (Fig. 12).

4. Theoretical model database and simulation for the ME (E = SWC6-MAX) unit performance under FF and variable pressure conditions with 3.2% NaCl feed

The theoretical database for the performance simulation of the SWRO-CCD ME (E = SWC6-MAX) unit displayed in Fig. 1 under FF and variable pressure conditions, described in Table 2, is intended for comparison with the related process under FP and variable flow conditions described in Table 1. Accordingly, in order to allow for a relevant comparison, the principle operational features in both table are selected to be the same including the number of CCD cycles (10), flow rate of CP (4.0 m^3/h), cycle duration (0.9 min/cycle), average sequential flux (14.9 lmh), feed source (3.2% NaCl), and temperature (25°C), and such a selection of parameters led to the same sequence duration (9.01 min) and sequence recovery (60.3%). The application of the FF theoretical database model for CCD-SWRO simulation was already disclosed and explained at length elsewhere [9,10] and shall be considered hereinafter mainly in relationship to the parallel CCD process under FP conditions outlined in Table 1. Performance correlation between the analogous FP and FF modes of operation of the same single-element unit design (ME: E = SWC6-MAX) according to the data disclosed in Tables 1 and 2 is discussed next.

5. Results and discussion

The recently reported SWRO-CCD method under FF and variable pressure conditions of high recovery

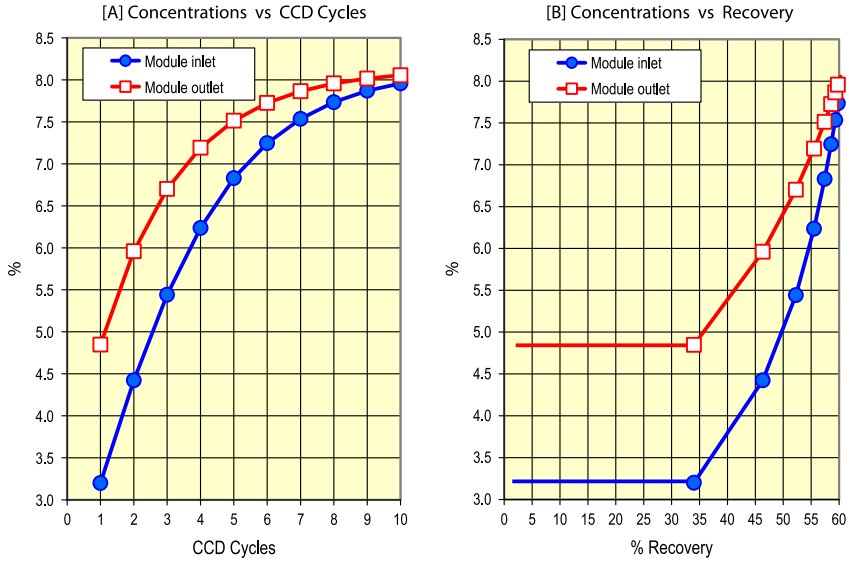

Fig. 3. Concentration variations at module inlet and outlet during the SWRO-CCD sequence under FP and variable flow conditions as function of CCD cycles (A) and recovery (B) for the single-element (SWC6-MAX) unit design in Fig. 1 according to the data in Table 1.

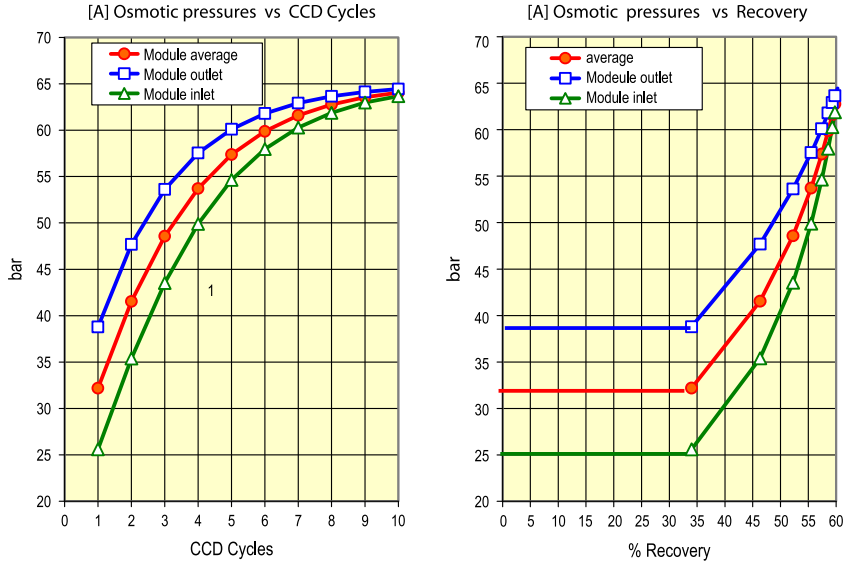

Fig. 4. Osmotic pressure variations at module inlet, outlet, and average during the SWRO-CCD sequence under FP and variable flow conditions as function of CCD cycles (A) and recovery (B) for the single-element (SWC6-MAX) unit design in Fig. 1 according to the data in Table 1.

and low energy without need of an ERD was characterized experimentally for units of MEn (n = 1–4) MEs with Mediterranean seawater, and the results [6–10] obtained revealed near-absolute energy efficiency and high consistency with theoretical model projections. The theoretical model simulation results for the SWRO-CCD ME (E = SWC6-MAX) unit under FF conditions disclosed in Table 2 are trustworthy since fully supported by relevant experimental data [6,7]. It should be pointed out that some very brief

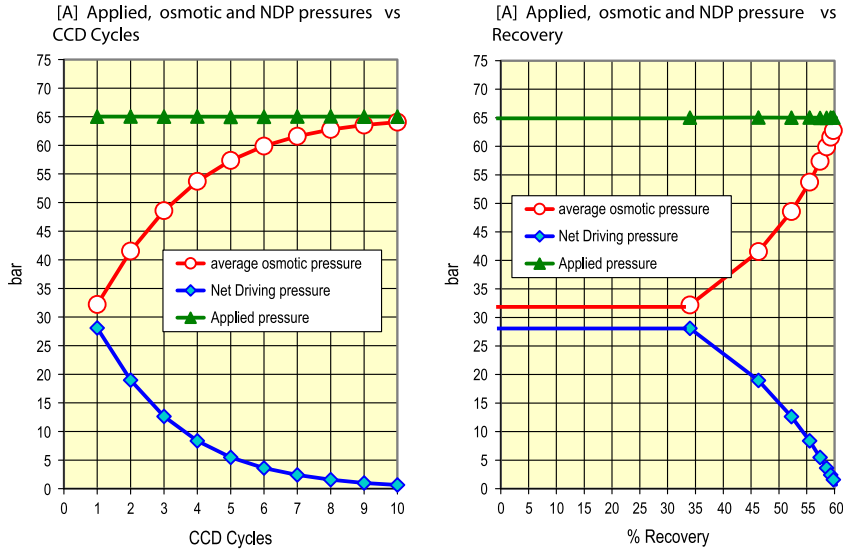

Fig. 5. Applied, osmotic, and NDP pressure variations during the SWRO-CCD sequence under FP and variable flow conditions as function of CCD cycles (A) and recovery (B) for the single-element (SWC6-MAX) unit design in Fig. 1 according to the data in Table 1.

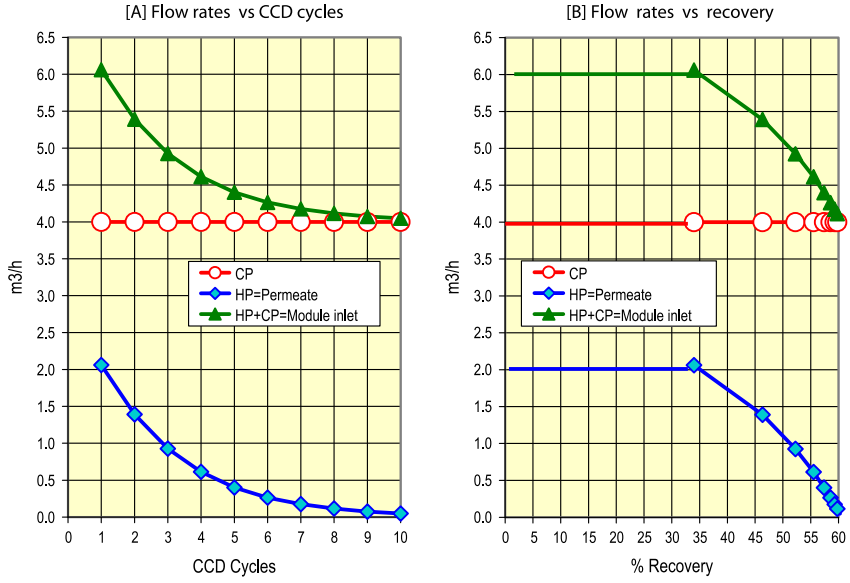

Fig. 6. Flow variations during the SWRO-CCD sequence under FP and variable flow conditions as function of CCD cycles (A) and recovery (B) for the single-element (SWC6-MAX) unit design in Fig. 1 according to the data in Table 1.

experimental trials with BWRO-CCD units comprising MEn (n = 3–4) modules were also performed under FP conditions apart from the normal FF operational mode, and confirmed the availability of such an operational option [13]. However, CCD under FP conditions was never explored any further and the present study provides for the first time, some noteworthy comparative theoretical model data of the FF and FP operational modes of CCD. While comparison between the RO energy consumption of conventional SWRO-PFD and SWRO-CCD requires assumption of the ERD efficiency in the former process [8], the present study circumvents entirely the issue of energy recovery since both CCD modes under FF and FP conditions are performed with the same apparatus of near-absolute energy efficiency without ERD using the

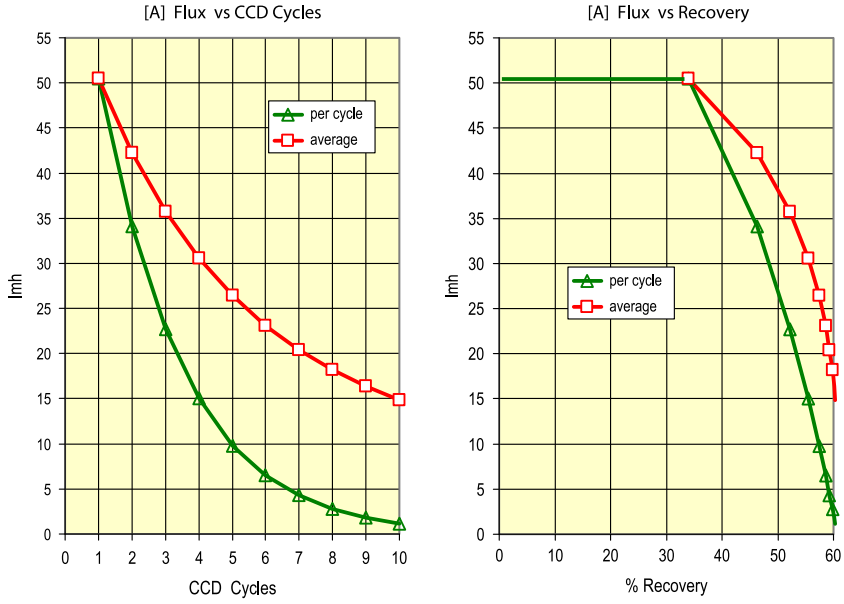

Fig. 7. Flux variations during the SWRO-CCD sequence under FP and variable flow conditions as function of CCD cycles (A) and recovery (B) for the single-element (SWC6-MAX) unit design in Fig. 1 according to the data in Table 1.

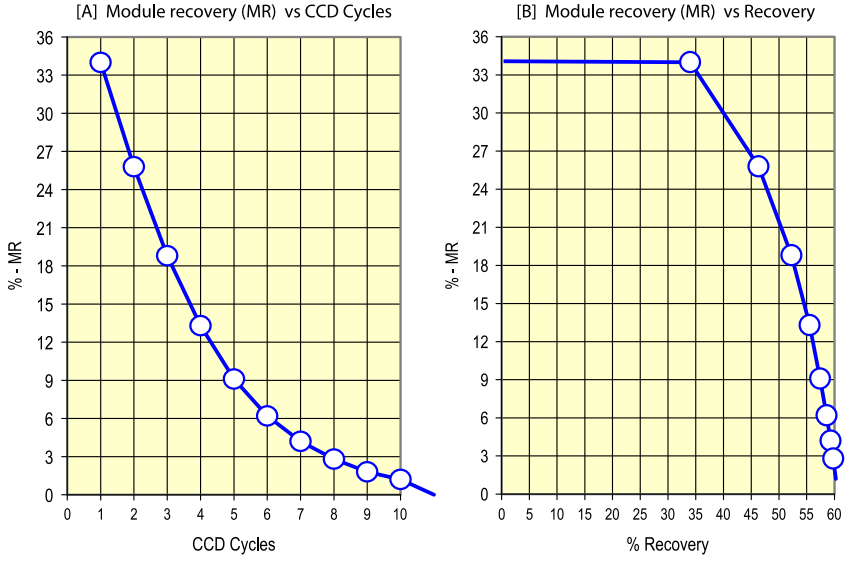

Fig. 8. Percent MR variations during the SWRO-CCD sequence under FP and variable flow conditions as function of CCD cycles (A) and recovery (B) for the single-element (SWC6-MAX) unit design in Fig. 1 according to the data in Table 1.

same feed source at the same temperature, average flux and recovery, and the energy requirements are defined solely on the basis of intrinsic features.

The FP (65 bar) theoretical model performance of the SWRO-CCD ME unit, revealed in Table 1, pertains to realistic conditions of 60.3% batch sequence recovery over 9.01 min by 10 CCD cycles of fixed interval (0.9 min/cycle) due to a fixed cross-flow (Qc_P = 4.0 m^3/h) under declined flux starting with 50.5 lmh (2.06 m^3/h permeate and/or HP pressurized feed), and module inlet flow (Q_{HP} + Q_{CP}) of 6.06 m^3/h which manifests MR = 34% and *pf* = 1.147. The first cycle-simulated conditions cited above, are consistent with the results of a converged IMS Design Program

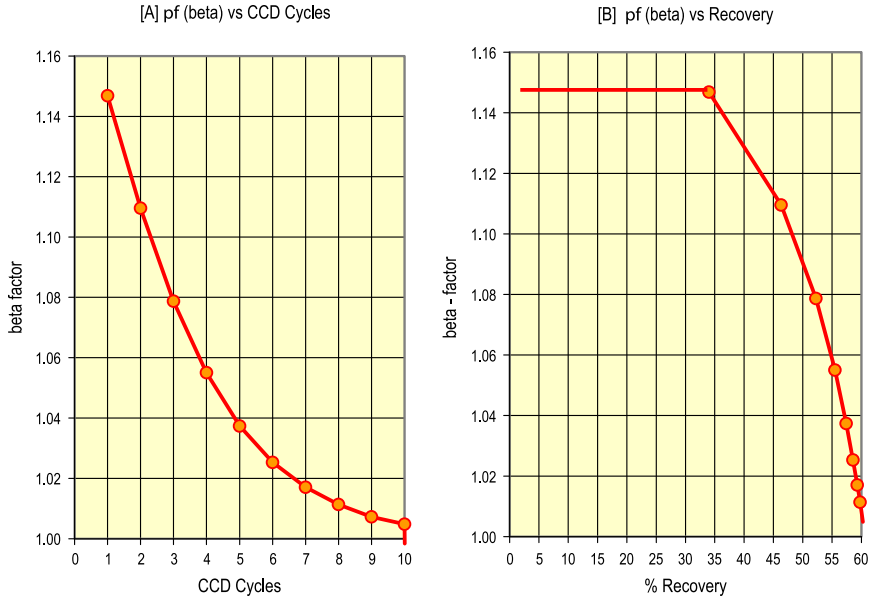

Fig. 9. Concentration polarization factor (beta) variations during the SWRO-CCD sequence under FP and variable flow conditions as function of CCD cycles (A) and recovery (B) for the single-element (SWC6-MAX) unit design in Fig. 1 according to the data in Table 1.

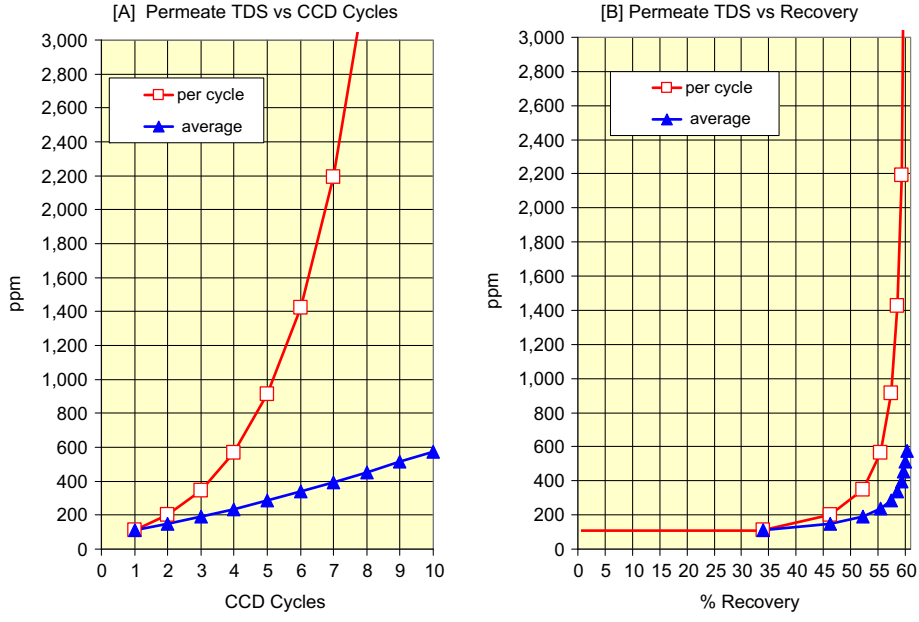

Fig. 10. Permeate TDS and average TDS variations during the SWRO-CCD sequence under FP and variable flow conditions as function of CCD cycles (A) and recovery (B) for the single-element (SWC6-MAX) unit design in Fig. 1 according to the data in Table 1.

for a single-SWC6-MAX element unit which reveals for feed of 3.2% NaCl, 63.5 bar applied pressure with beta factor of 1.15 for permeate flow of 2.1 m^3/h and 33% recovery. The permeate flow (2.06 m^3/h) of the initial cycle is essentially that cited [12] in the performance data of the SWC6-MAX element (50 m^3/day). The sequence progression described in Table 1, beyond the first cycle, is dictated by the module concentration variations, and the declined MR and flux are required to sustain the FP (65 bar) mode of operation.

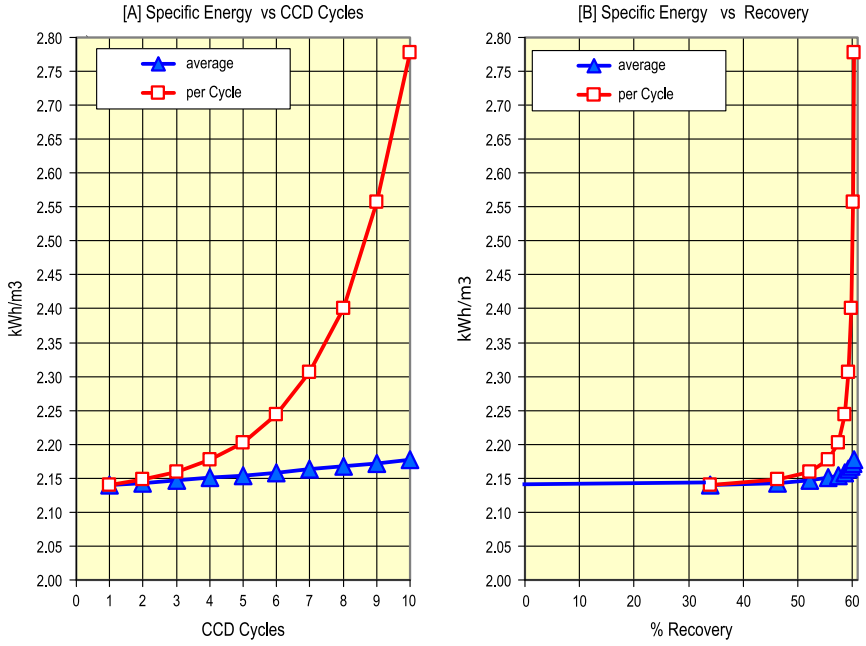

Fig. 11. SE variations during the SWRO-CCD sequence under FP and variable flow conditions as function of CCD cycles (A) and recovery (B) for the single-element (SWC6-MAX) unit design in Fig. 1 according to the data in Table 1.

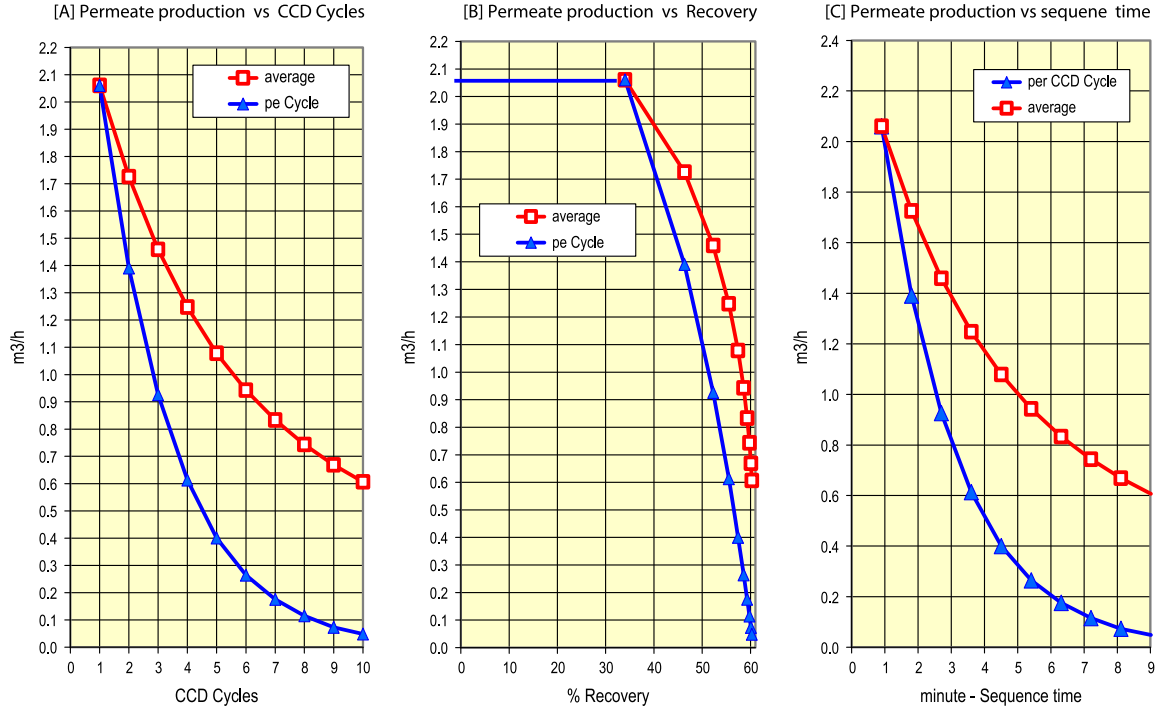

Fig. 12. Permeate production rates during the SWRO-CCD sequence under FP and variable flow conditions as function of CCD cycles (A), recovery (B) and sequence time (C) for the single-element (SWC6-MAX) unit design in Fig. 1 according to the data in Table 1.

Table 2
Theoretical model database for the simulated performance of the single-element SWCO-CCD ME (E = SWC6-MAX) unit under FF and variable applied pressure conditions with a feed of 3.2% NaCl equivalent to typical Ocean seawater of 35,000 ppm at 25℃, 14.9 lmh fixed flux, MR = 10%, and constant CP flow rate (4.0 m^3/h)

TEST - SWC6 MAX		UNIT DESIGN		CCD Parameters		Temperature	
40.8	m2/Element	1	Modules	3.20	% Initial feed	≥25 25	°C
50	m3/day	1	Elements/Module	14.9	lmh Flux	≥25 1.000	TCF
32,000	ppm NaCl	230	cm long PV	0.61	m3/h Permeate (=Q_{HP})		
54	bar Applied Pressure	20	cm diameter PV	13.2	% Module Recovery	≤25 25	°C
10	% Recovery	15	liter element volume	4.00	m^3/h Qcp	≤25 1.000	TCF
25	Centigrade	5	% lines volume	4.61	m^3/h Module Inlet flow		
99.70	% Salt Rejection	60.1	liter per module	0.08	bar Δp		
28.4	bar NDP			0.90	min/cycle CCD		
51.062	l/m2/h Flux	π(bar)-C(%)		0.0091	m3/cycle of permeate	Pumps	
1.798	l/m2/h/bar -A	32,000	ppm NaCl Feed	0.132	av-MR/Element-CCD	0.85	HP *eff*.
0.1203	l/m2/h - B	25.60	bar Osmotic Pressure	1.047	*av-pf* - CCD	0.75	CP *eff*.
		8.00	π(bar)/C(%)	7.59	Flow ratio(concentrate/permeate)		

FIXED FLOW VARIABLE PRESSURE SWRO-CCD SINGLE ELEMENT MODULE PERFORMANCE

Steps & Concentrations				CCD Sequence Cycles							CCD Sequence Combined				Permeate	
		Inlet	Outlet	Time	Applied (p_a)		POWER (kW)			SE		avergae		REC	Cycle	average
Mode	Step	%	%	min	bar	av-bar	HP	CP	HP+CP	kWh/m3	Σm3	ΣkW	kWh/m3	%	ppm	ppm
CCD	1	3.20	3.69	0.90	37.1	37.1	0.736	0.012	0.749	1.234	0.009	0.749	1.234	13.2	291	291
CCD	2	3.62	4.17	1.80	40.9	39.0	0.812	0.012	0.824	1.358	0.018	0.786	1.296	23.3	330	311
CCD	3	4.04	4.66	2.70	44.7	40.9	0.887	0.012	0.899	1.482	0.027	0.824	1.358	31.3	368	330
CCD	4	4.46	5.14	3.60	48.5	42.8	0.962	0.012	0.974	1.606	0.036	0.861	1.420	37.8	407	349
CCD	5	4.89	5.63	4.51	52.3	44.7	1.037	0.012	1.050	1.730	0.046	0.899	1.482	43.1	445	368
CCD	6	5.31	6.11	5.41	56.1	46.6	1.113	0.012	1.125	1.854	0.055	0.937	1.544	47.6	483	387
CCD	7	5.73	6.60	6.31	59.9	48.5	1.188	0.012	1.200	1.978	0.064	0.974	1.606	51.5	522	407
CCD	8	6.15	7.08	7.21	63.7	50.4	1.263	0.012	1.275	2.102	0.073	1.012	1.668	54.8	560	426
CCD	9	6.57	7.57	8.11	67.5	52.3	1.338	0.012	1.351	2.226	0.082	1.050	1.730	57.7	599	445
CCD	10	6.99	8.05	9.01	71.3	54.2	1.414	0.012	1.426	2.350	0.091	1.087	1.792	60.3	637	464

The batch sequence performance characteristics of the SWRO-CCD-FP ME (E-SWC6-MAX) model unit are displayed in Figs. 3(A) and (B) to 12(A) and (B) as functions of CCD cycles (henceforth labeled "A") and recovery (henceforth labeled "B"). Fig. 3(A) and (B) describes module inlet and outlet feed concentrations per cycle which take into account the dilution effect of recycled concentrates with feed as function of declined MR. The flow ratio relationship $Q_{HP}/Q_{CP} = Q_P/Q_{CP} = MR/(100 - MR)$ derived from Eq. (1) manifests the dilution effect and implies the concomitance of the sequentially declined MR with a smaller gap between inlet and outlet module concentrations as evident in Fig. 3(A) and (B). Increased module concentrations during the sequence progression with a declined dilution effect are also manifested by the module osmotic pressure variations revealed in Fig. 4(A) and (B). The pressure characteristics of the CCD FP operational mode under review are evident in Fig. 5(A) and (B) by a fixed applied pressure coupled with increased average osmotic pressure of declined NDP during the batch sequential progression. The flow characteristics of the CCD FP system under review are evident in Fig. 6(A) and (B) by a fixed CP flow rate coupled with declined flow rates of HP, permeation, and module inlet during the batch sequential progression. The flux variations per cycle and average in the system under review, revealed in Fig. 7(A) and (B), are noteworthy in particular, since flux is part of the applied pressure (p_a) expression (Eq. (2)) and therefore, are principle component of the power expression (Eq. (11)) and major contributors to the SE term as defined by Eq. (14). Apart from its major impact on pressure and energy, flux is also a dominant factor in the salt rejection expression (Eq. (10)) which defines the TDS of permeates. The declined flux pattern observed in Fig. 7(A) and (B) is typical of a CCD-FP batch sequential process and the average flux (~15 lmh) over the entire sequence of 10 cycles of 60.3% recovery characterizes the average performance of the entire sequence. The declined sequential MR displayed in Fig. 8(A) and (B) is essential to sustain the fixed applied pressure mode of operation and also dictates (Eq. (3): $Y = MR/100$) the declined concentration polarization factor (*pf* or beta) revealed in Fig. 9(A) and (B) which applies for $\Delta\pi_{av}$ calculation as well as in the salt rejection expression Eq. (10).

The ultimate performance characteristics of a batch sequential CCD process irrespective of its mode of operation are determined by the recovery (%), SE (kWh/m^3), quality of permeates (ppm TDS), and production rate (m^3/h), and these aspects in the context of the SWRO-CCD-FP ME (E = SWC6-MAX) model unit are considered next and disclosed in Figs. 10(A) and (B) to 12(A) and (B). In contrast with conventional SWRO-PFD units with modules of 7–8 elements which are confined to 45–50% recovery at and an average flux of 13–15 lmh, the performance of the single-element FP model unit under review proceeds by 10 cycles of 60.3% recovery with the average values of flux (14.9 lmh), SE (2.177 kWh/m^3), permeates TDS (574 ppm), and permeate productivity (0.61 m^3/h) indicated in parentheses. Permeate TDS per cycle derived by Eq. (10) is inversely proportional to flux and directly proportional to the module feed concentration (C_f) which explains the fast rise of TDS per cycle revealed in Fig. 10. The average TDS, which also takes into account the fraction of permeate volume production per cycle apart from TDS, shows a fast exponent rise only beyond the 55% recovery level (Fig. 10B). The SE variation patterns per cycle and average in the model system under review (Fig. 11(A) and (B)) appear to be similar to those revealed for permeates' TDS (Fig. 10(A) and (B)) with a fast exponent rise of SE per cycle only beyond the 55% recovery level (2.140–2.778 kWh/m^3) of expected small effect on the average (2.140–2.177 kWh/m^3) since the fast exponential rise originates from the rapidly declined permeate volume production per cycle of decreased effect on the overall. Permeate productivity (m^3/h) in the model system under review is disclosed in Fig. 12(A)–(C) as a function of CCD cycle (A), recovery (B), and batch sequence time progression (C), and shows an average of 0.61 m^3/h per batch sequence 9.01-min long 14.9 lmh of average flux with 2.177 kWh/m^3 average SE and such performance data is unattainable by the average element of the conventional PFD techniques.

The theoretical model performance analysis of the same SWRO-CCD ME unit (Fig. 1) with the same feed source under FF and FP conditions is of interest since it enables to follow intrinsic process variations of two different CCD modes, both of near-absolute energy efficiency. According to Fig. 13(A) and (B), both compared modes (FF and FP) proceed with the same sequence recovery (60.3%) and number of CCD cycles (10) over the same period duration (9.01 min) and reach the same average flux (14.9 lmh) at the end of the batch sequence (Fig. 14(A) and (B)). The flow pattern of both modes in Fig. 15(A) and (B) reveal identical CP recycling rates (Q_{CP} = 4.0 m^3/h) with HP flow rate (Q_{HP}) under FF conditions remains unchanged; whereas, that under FP conditions, declines with sequence progression. Flow rates of HP displayed in Fig. 15(A) and (B) are equivalent to flow rates of permeates since under CCD conditions $Q_{HP} = Q_P$. Permeate and/or HP flow rates in the compared systems are a function of MR (Fig. 16(A) and (B)) which is maintained constant under FF of variable

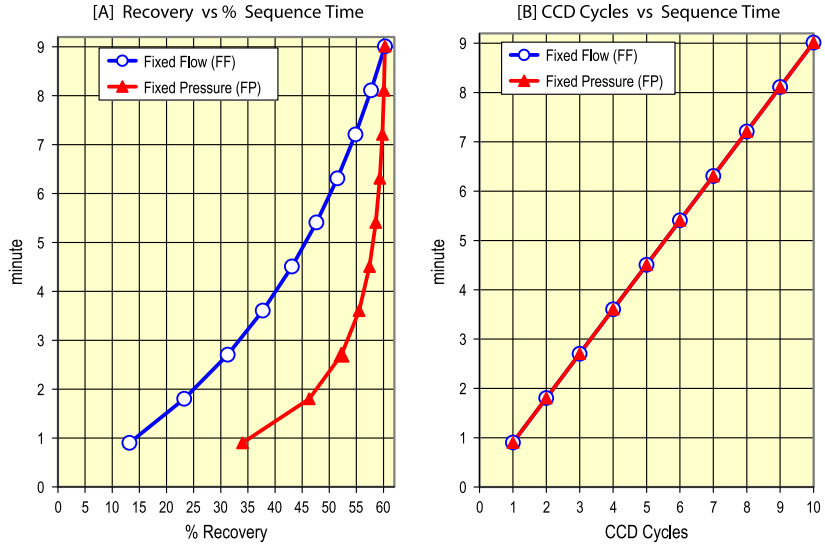

Fig. 13. Sequence time progression as function recovery (A) and CCD cycles (B) under the FP and FF operational conditions by the same SWRO-CCD ME (E = SWC6-MAX) unit design (Fig. 1) according to data disclosed in Table 1 (FP) and Table 2 (FF).

pressure and changes during the batch sequence progression under FP and variable flow conditions in order to enable a constant pressure operation.

A noteworthy distinction between performance of the SWRO-CCD ME model unit under FF and FP conditions at the same average flux (14.9 lmh) relates to applied pressures (Fig. 17(A) and (B)) and SEs (Fig. 18(A) and (B)). Pressure profiles revealed in Fig. 17(A) and (B) are of constant pressure (65 bar) during the FP mode and changing pressure per cycle and average during the FF mode with exponential relationship on the recovery scale (Fig. 17(A)) and linear relationship on the CCD cycles scale (Fig. 17(B)). Most of the SE in CCD, irrespective of mode, is a function of the average sequential pressure since $Q_P = Q_{HP}$ and this is manifested amongst others by the pattern similarity between the pressure curves in Fig. 17(A) and (B) and the SE curves Fig 18(A) and (B). A noteworthy result of this theoretical model study is the SE difference (0.385 kWh/m^3) of the compared FF (2.177 kWh/m^3) and FP (1.792 kWh/m^3) batch processes of the same time duration (9.01 min), recovery (60.3%), and average flux (14.9 lmh). In simple terms, under the specified conditions, the RO energy for FF is found to be 17.7% lower than that of the analogous FP process. The average SE difference and percent energy saved by FF compared with FP (in parenthesis) as function of recovery (R) in the context of the model study under review are found to be as follows: R = 40%, 0.692 (32.3%); R = 45%, 0.643 (30.1%); R = 50%, 0.567 (26.4%); R = 55%, 0.471 (21.9%); and R = 60.3%, 0.385 kWh/m^3 (17.7% energy saving). Assuming that the SWRO-CCD-FP model under review for 3.2% NaCl feed is related to a conventional SWRO-PFD process for Ocean seawater of 65 bar applied pressure, average flux of 14.9 lmh and recovery of 50%, the aforementioned may suggest the saving of at least 26.4% of the energy using the SWRO-CCD-FF process instead of conventional SWRO-PFD with EDR. This conclusion is consistent with the reported [14] RO energy of the Perth conventional desalination plant in Australia (2.46 kWh/m^3) when compared with the extrapolated normalized value (~1.70 kWh/m^3) [15,16] derived from experimental SWRO-CCD-FF results [6,7] for Mediterranean seawater which reveals ~31% energy saving by the latter. The Perth example is just one of many which reveals the RO energy range 2.46–3.5 kWh/m^3 for large advanced desalination plants operated with Mediterranean (~40,000 ppm) seawater [3,17,18] and Ocean (~35,000 ppm) seawater [3,14] whose energy aspects are discussed elsewhere [8].

Seawater RO desalination is an energy-rich process of growing importance for domestic water supplies worldwide in light of the rapid depletion of natural water sources, and the saving of energy by the RO process has been viewed as a major objective [3] of the growing desalination industry. The SWRO-CCD-FF technology enables already today major savings of desalination energy costs not possible by conventional techniques.

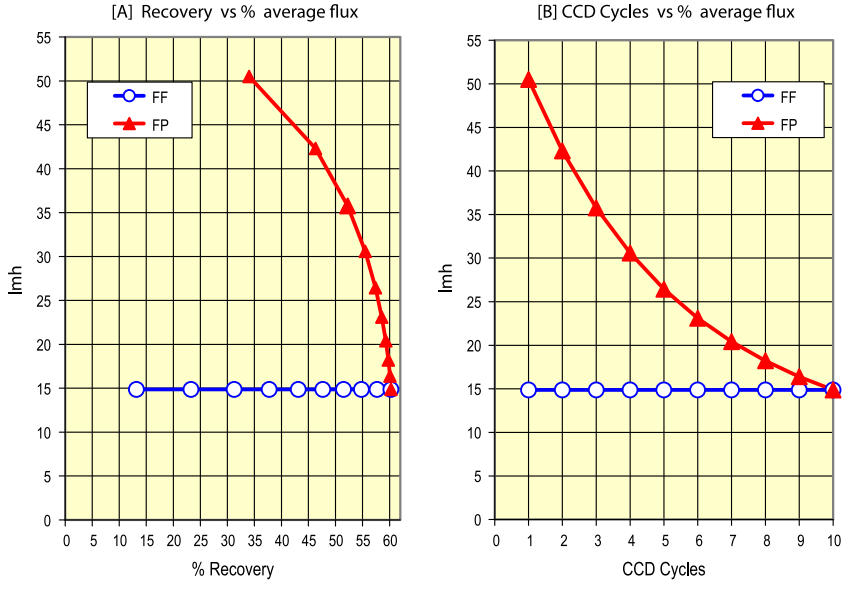

Fig. 14. Average flux during sequence progression as function recovery (A) and CCD cycles (B) under the FP and FF operational conditions by the same SWRO-CCD ME (E = SWC6-MAX) unit design (Fig. 1) according to data disclosed in Table 1 (FP) and Table 2 (FF).

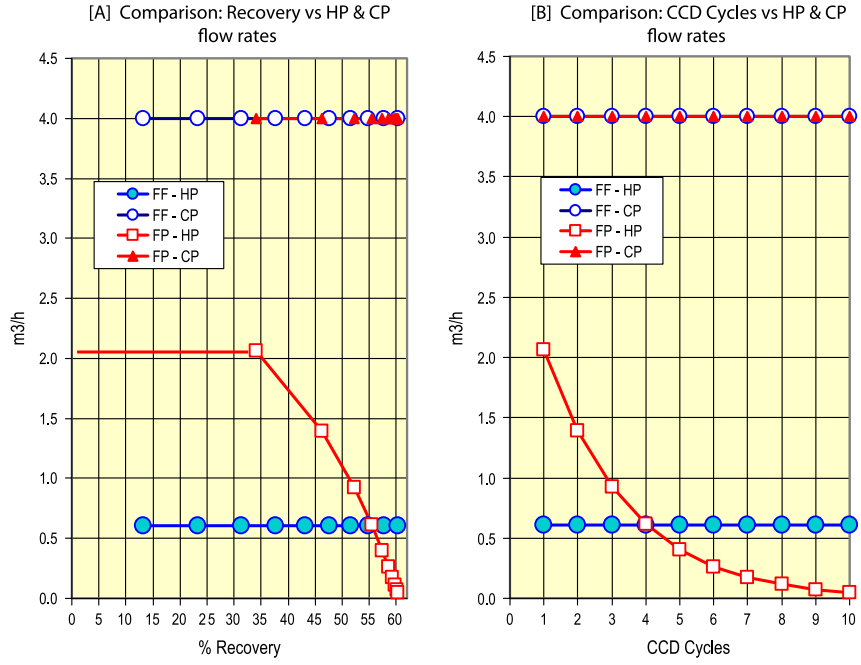

Fig. 15. Flow pattern during sequence progression as function recovery (A) and CCD cycles (B) under the FP and FF operational conditions by the same SWRO-CCD ME (E = SWC6-MAX) unit design (Fig. 1) according to data disclosed in Table 1 (FP) and Table 2 (FF).

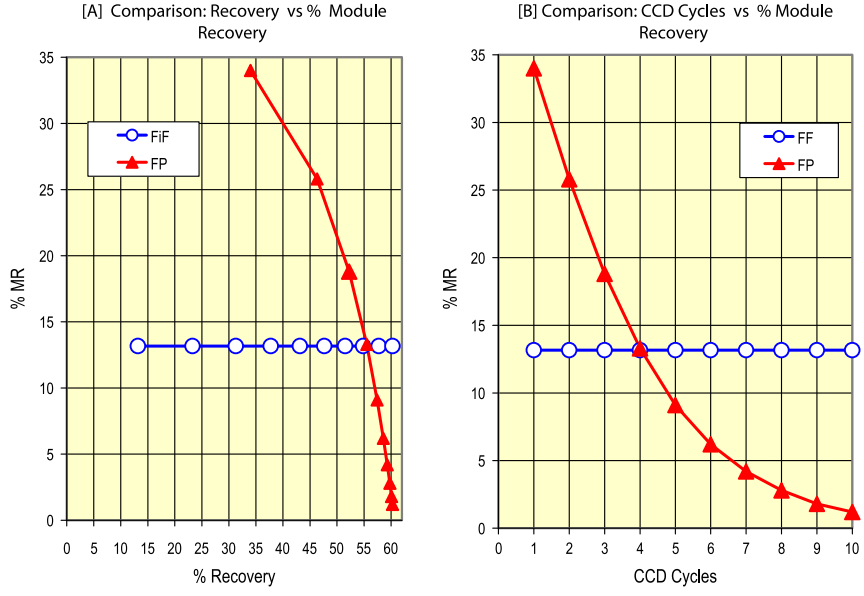

Fig. 16. MR during sequence progression as function recovery (A) and CCD cycles (B) under the FP and FF operational conditions by the same SWRO-CCD ME (E = SWC6-MAX) unit design (Fig. 1) according to data disclosed in Table 1 (FP) and Table 2 (FF).

The theoretical model performance of the SWRO-CCD ME unit under the FF and FP conditions is revealed in Fig. 19(A) and (B) in terms of TDS (ppm) of permeates per cycle according to Eq. (10) as well as average TDS of permeates during the batch sequence accumulation expressed by mass (ppm) and volume. The different TDS patterns under FF and FP conditions manifest the fixed flux irrespective of CCD

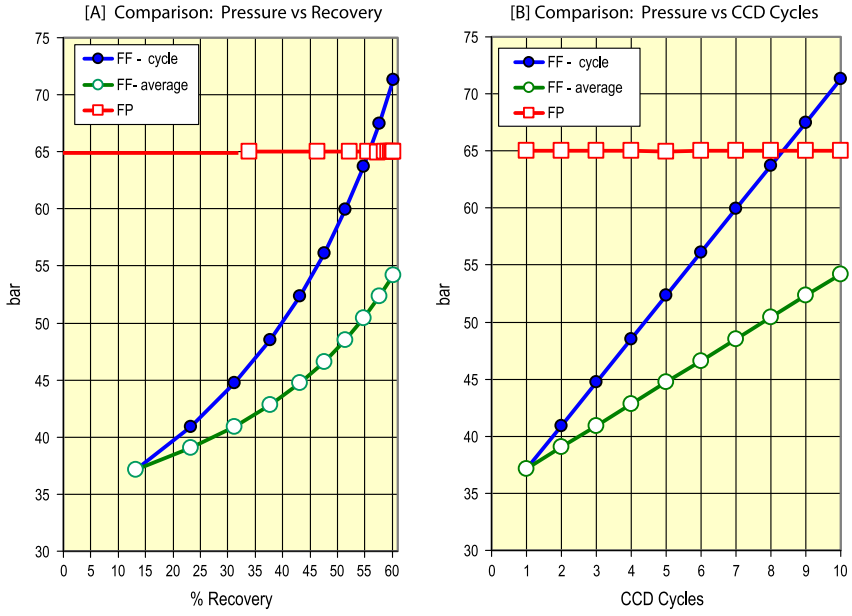

Fig. 17. Applied pressure during sequence progression as function recovery (A) and CCD cycles (B) under the FP and FF operational conditions by the same SWRO-CCD ME (E = SWC6-MAX) unit design (Fig. 1) according to data disclosed in Table 1 (FP) and Table 2 (FF).

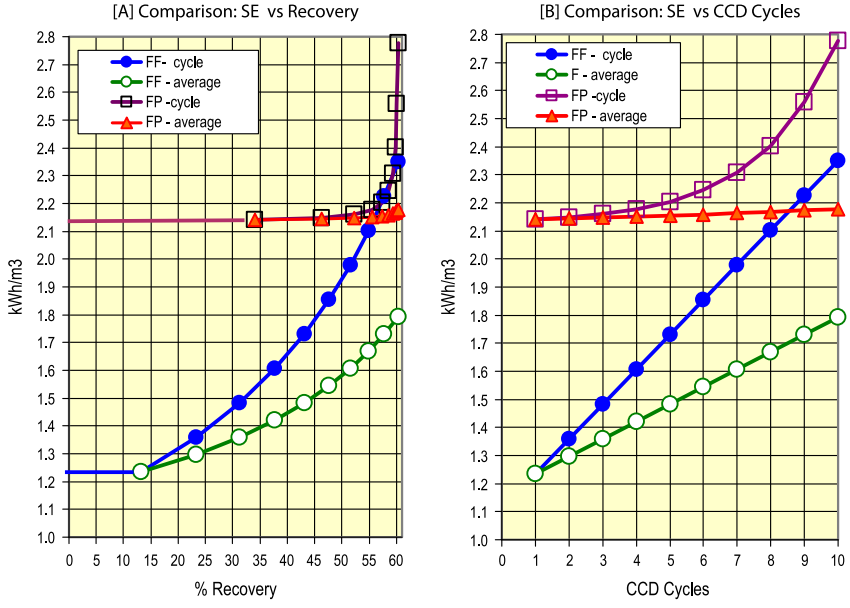

Fig. 18. SE during sequence progression as function recovery (A) and CCD cycles (B) under the FP and FF operational conditions by the same SWRO-CCD ME (E = SWC6-MAX) unit design (Fig. 1) according to data disclosed in Table 1 (FP) and Table 2 (FF).

cycle in the former process and the declined flux per cycle in the latter process. Fixed-flux (FF) operation according to Eq. (10) implies the dependence of TDS mainly on the recycled flow concentration (C_f), whereas under FP conditions, the declined flux becomes another important parameter in the said equation, effecting fast increase of TDS with declined flux. The flux effect on TDS under FP conditions in evident by the fast exponential rise per CCD cycle in Fig. 19(A) as well as on the recovery scale in

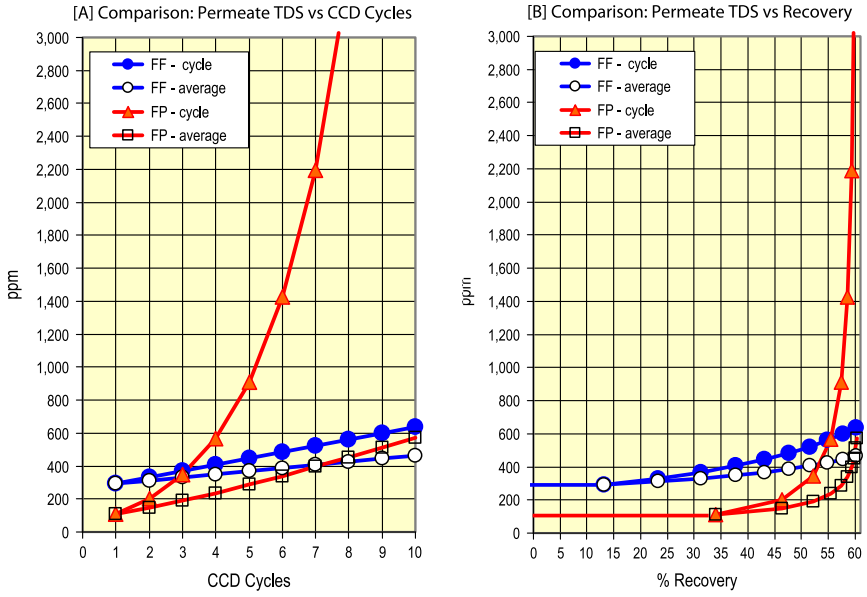

Fig. 19. TDS of permeates during sequence progression as function recovery (A) and CCD cycles (B) under the FP and FF operational conditions by the same SWRO-CCD ME (E = SWC6-MAX) unit design (Fig. 1) according to data disclosed in Table 1 (FP) and Table 2 (FF).

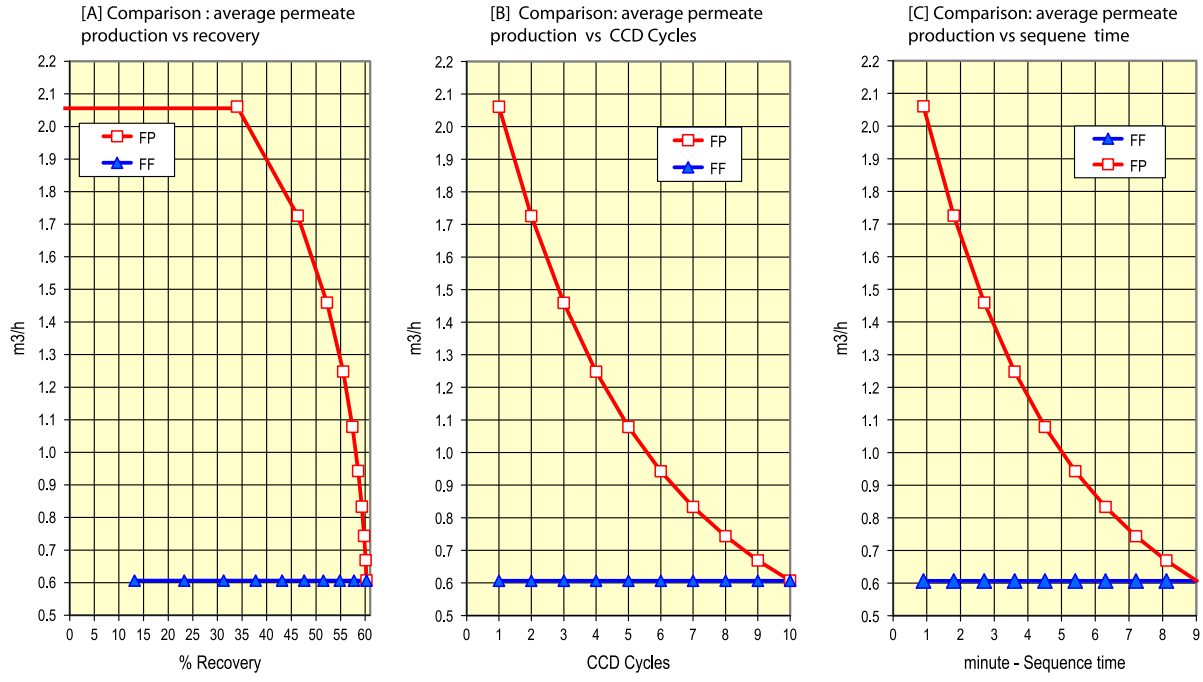

Fig. 20. Average permeate production during sequence progression as function recovery (A), CCD cycles (B), and time-scale (C) under the FP and FF operational conditions by the same SWRO-CCD ME (E = SWC6-MAX) unit design (Fig. 1) according to data disclosed in Table 1 (FP) and Table 2 (FF).

Fig. 19(B) above 50% recovery. The average TDS (ppm) of permeates at the end of the compared CCD batch processes of same time duration (9.01 min), recovery (60.3%), and average flux (14.9 lmh) are 574 ppm for FP and 464 ppm for FF. However, Fig. 19(B) also reveals better average quality permeates

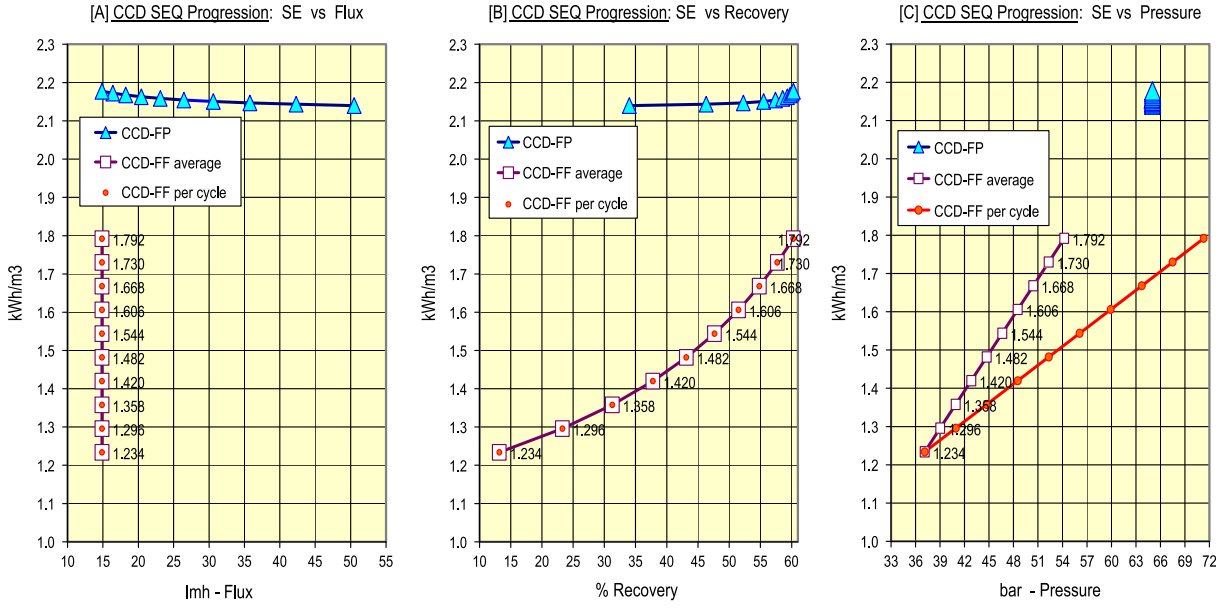

Fig. 21. SE sequential variations as function of flux (A), recovery (B), and applied pressure (C) during the FF and FP operations of the same SWRO-CCD ME (E = SWC6-MAX) unit design (Fig. 1) according to data disclosed in Table 1 (FP) and Table 2 (FF).

under FP compared with FF below ~54% recovery and the tendency changes above this recovery level due to the very high exponential rise of TDS per cycle in the FP process. Incidentally, the region of large TDS exponential rise per cycle in the FP process is associated with a rapidly declined flux of diminished permeate volume production manifested by relatively small variations in the average TDS of the process.

Another aspect of the compared FP and FF CCD processes relates to the permeate productivity rates disclosed in Fig. 20(A)–(C) in reference to recovery (A), CCD cycles (B), and sequence duration (C). Evidentially, the average and per cycle permeate production during the FF process are the same (0.61 m^3/h) since generated under fixed flux, MR, and NDP conditions; whereas, the average and per cycle permeate production during the FP process vary continuously as function of the changing flux, MR, and NDP. The average permeate production rates of the compared FF and FP processes become the same at the same average flux manifested in the latter at the end of the batch sequence (14.9 lmh).

6. Concluding remarks and summary

The newly emerging CCD technology originated from theoretical model simulation and validated experimentally with projections and results agree within ±2%. The computer design programs of commercial CCD systems make use of the original theoretical model concepts for performance projections of plants with considerable success. The conceptual model principles of CCD are based on consecutive sequential batch desalination processes of fixed flux created under FF and variable pressure conditions with near-absolute energy efficiency without the need for ERD. The theoretical model performance comparison of the same SWRO-CCD ME unit under FP and FF conditions described hereinabove reveals the preference of the FF mode of operation over FP for reasons as follows:

(1) Lower SE for same sequence duration, recovery, average flux, and average production rate of permeates of similar average TDS.
(2) Fixed NDP through the CCD sequence of a uniform constant pressure difference across membrane surfaces for prevention of their motion.
(3) Flexible selection flow rates set points of pressurized feed (Q_{HP}), permeate (Q_P) or flux, and cross-flow (Q_{CP}).
(4) MR control through the selected set points of flow rates independent of maximum applied pressure and/or sequence recovery.
(5) Sequence recovery determined by set point of maximum applied pressure and/or maximum electric conductivity of recycled concentrates, irrespective of flow rates, flux, and MR selection.

The most dramatic difference between the compared FP and FF processes under review pertains to the SE variations revealed in Fig. 21 as function of flux (A), recovery (B), and applied pressure (C). The SE progression of 1.234–1.792 kWh/m^3 for FF compared with 2.140–2.177 kWh/m^3 for FP of the same sequence duration (9.01 min) and recovery (60.3%) are viewed with respect to each other in Fig. 21 on different scales as follows: SE vs. Flux disclosed in Fig. 19(A) reveals that FF is carried out at the same flux with increased SE; whereas, FP is associated with a much greater SE of small variability with flux. Increased SE in FF under fixed flux takes place as function of recovery (Fig. 21(B)) manifested by increased applied pressure (Fig. 21(C)); whereas in case of FP, very small SE variations are encountered with recovery and applied pressure. Most of the CCD energy requirements are related to the pressurizing pump (HP) and the SE contribution of this pump is only a function of pressure and expressed by $SE_{HP} = p_a/36/\text{eff}$ since $Q_{HP} = Q_P$. In simple terms, the SE_{HP} contribution under FP conditions with average applied pressure of 65 bar is expressed by $SE_{HP\text{-}FP} = 1.8055/\text{eff}$ kWh/m^3; whereas, the same term under FF conditions with an average applied pressure of 54.2 bar is expressed by $SE_{HP\text{-}FF} = 1.505/\text{eff}$ kWh/m^3 and the ratio $SE_{HP\text{-}FF}/SE_{HP\text{-}FP} = 0.833$ for the same pump efficiency ratio (eff) manifests 16.7% saving by FF compared with FP for batch of 60.3% recovery. Comparison of the total SE, instead of only SE_{HP}, discussed already hereinabove revealed even higher energy savings of 17.7% instead of 16.7%. The energy-saving aspect of CCD under FF compared with FP conditions is traced to the average applied pressure increase with recovery by the former not possible by neither latter nor by conventional SWRO which also takes place with fixed applied pressure. Conventional SWRO is a PFD process performed inside long pressure vessels of 7–8 elements with fixed applied pressure, declined flux, need for ERD to achieve energetic efficiency, and without any feed dilution effect between successive elements as in the case of CCD. SE comparison of conventional SWRO-PFD and SWRO-CCD-FP should manifest the benefits of the latter with respect to its near-absolute energy efficiency without need of ERD. SE comparison of conventional SWRO-PFD and SWRO-CCD-FP should also reveal the benefits of the latter with respect to its near-absolute energy efficiency without need of ERD. SE comparison of conventional SWRO-PFD and SWRO-CCD-FF also manifests the gradual average applied pressure requirements and the dilution effect at inlet to pressure vessels in the latter whereby further energy savings are encountered.

The theoretical model comparison of the single-element SWRO-CCD unit under FF and FP conditions described hereinabove is noteworthy also in the context of the recent US patent application by Tarquin [11] entitled "Sea water reverse osmosis systems to reduce concentrate volume prior to disposal"; wherein, an open-circuit SWRO-PFD-FP apparatus with single-element modules is demonstrated for effective volume reduction of high-silica concentrates. The plausible use of SWRO-CCD units comprising short MEn (n = 1–3) modules for effluent volume reduction with rescued water for reuse is also suggested by the current study.

Acknowledgments

Funds to *Desalitech Ltd*. by AQUAGRO FUND L.P. (Israel) and by Liberation Capital LLC (USA) are gratefully acknowledged.

References

[1] S. Loeb, S. Sourirajan, sea water demineralization by means of an osmotic membrane, American Chemical Society Advances in Chemistry Series ACS 38 (1963) 117–132.
[2] M. Elimelech, W.A. Phillip, The future of seawater desalination: Energy, technology, and the environment, Science 333 (2011) 712–717.
[3] N. Voutchkov, Membrane seawater desalination—Overview and recent trends, IDA Conference, November 2–3, 2010, Huntington Beach, CA.
[4] Status document "Desalination a national perspective" sponsored by the National Research Council of the National Academies, National Academies Press, Washington, DC, 2008. Available from: http://www.nap.edu/catalog/12184.html.
[5] Design and practical aspects of RO are considered in manuals of all major membranes producers as exemplified by "Dow Liquid Separation, FILMTEC™ Reverse Osmosis Membranes, Technical Manual", 2011. Available from: http://msdssearch.dow.com.
[6] A. Efraty, R.N. Barak, Z. Gal, Closed circuit desalination—A new low energy high recovery technology without energy recovery, Desalin. Water Treat. 31 (2011) 95–101.
[7] A. Efraty, R.N. Barak, Z. Gal, Closed circuit desalination series no-2: New affordable technology for sea water desalination of low energy and high flux using short modules without need of energy recovery, Desalin. Water Treat. 42 (2012) 189–196.
[8] A. Efraty, Closed circuit desalination series no-6: Conventional RO compared with the conceptually different new closed circuit desalination technology, Desalin. Water Treat. 41 (2012) 279–295.
[9] A. Efraty, Closed circuit desalination series no-8: Record saving of RO energy by SWRO-CCD without need of energy recovery, Desalin. Water Treat. (in press). 9 CCD Series No-8 online. doi: 10.1080/19443994.2013.822628.

[10] A. Efraty, CCD series no-11: Single module compact SWRO-CCD units of low energy and high recovery for seawater desalination including with solar panels and wind turbines, Desalin. Water Treat. (in press). CCD Series No-11 online. doi: 10.1080/19443994.2013.86203.
[11] A.J. Tarquin, Sea water reverse osmosis systems to reduce concentrate volume prior to disposal, US Patent Application, Pub. No.: US 2011/0036775 A1.
[12] Specifications of the SWC6-MAX membrane element by Hydranautics. Available from: http://www.memranes.com/docs/8inch/SWC6MAX.pdf.
[13] Unpublished results of *Desalitech* Ltd.
[14] M.A. Sanz, R.L. Stover, Low energy consumption in the Perth seawater desalination plant, IDA World Congress-Maspalomas, October 21–26, 2007, Gran Canaria—Spain, MP07.
[15] R.L. Stover, N. Efraty, Record low energy consumption with closed circuit desalination, IDA World Congress—Perth Convention and Exhibition Center (PCEC), September 4–9, 2011, Perth, Western Australia, REF: IDAWC/PER11-375.
[16] R.L. Stover, N. Efraty, Low energy consumption with closed circuit desalination, IDA J. Desalin. Water Reuse 4 (3) (2012) 12–19.
[17] B. Liberman, Present and future: Energy efficiency seawater desalination, IDA Conference, November 2–3, 2010, Huntington Beach, CA.
[18] A. Hermoni, Actual energy consumption and water cost for the SWRO systems at Palmachim—Case history, IDA Conference, November 2–3, 2010, Huntington Beach, CA.